Influence of miniband widths and interface disorder on vertical transport in superlattices

F. Piazza and L. Pavesi

Dipartimento di Fisica, Università di Trento, I-38050 Povo, Trento, Italy

A. Vinattieri, J. Martinez-Pastor,* and M. Colocci

Laboratorio LENS and Dipartimento di Fisica, Università di Firenze, I-50125 Firenze, Italy
(Received 8 July 1992; revised manuscript received 25 November 1992)

The nature of transport through superlattice minibands is addressed in this paper. All-optical techniques have been used to study the vertical transport, monitoring the luminescence from an enlarged well grown within the superlattice. Photoluminescence, photoluminescence excitation spectroscopy, and time-resolved luminescence-decay measurements have been performed as a function of temperature and excitation intensity. A consistent picture emerges from the experimental data, showing the key role played by the superlattice miniband widths and interface disorder on the vertical transport at low temperatures (4–40 K).

I. INTRODUCTION

Superlattices have intermediate properties between three-dimensional systems (bulk material) and quasi-two-dimensional systems (quantum wells). Their energy dispersion is typical of strongly anisotropic three-dimensional solids. The motion in the layer plane is characterized by free-carrier properties, while energy minibands are formed in the growth direction (let us call it vertical direction) having widths approximately one order of magnitude lower than the typical bandwidths in solids. Due to the formation of minibands, vertical transport occurs.

Vertical transport via miniband states has been studied by optical techniques since 1985, given the advantages of the higher spectral and temporal resolutions that optical techniques provide compared with ordinary electrical techniques.[1] The idea is the introduction of an enlarged well (EW), which is larger than those of the superlattice (SL), which acts as a spatial marker for the arrival of the carriers. It was realized that the carrier mobility through the superlattice is very sensitive to the miniband width and to the effective mass of the moving particles.[2,3]

Different transport regimes have been observed; whenever the particle mean free path is longer than the superlattice period, Bloch conduction occurs, whereas hopping diffusion assisted by phonons settles in if the particle mean free path is less than the SL period. Disorder strongly affects the vertical transport through the formation of localized (states that do not transport) and extended states inside the superlattice minibands.[4,5]

Further complications arise at low e-h pair densities from exciton formation. Excitonic effects have been normally avoided in vertical transport studies by performing measurements at high lattice temperatures, where excitons are thermally dissociated.[6,7]

The aim of this paper is to study the vertical transport in a set of nominally undoped superlattices at low temperatures ($T \leq 40$ K), where excitonic effects should play a non-negligible role. Photoluminescence techniques, continuous as well as time resolved, have been used and a consistent picture has been obtained from the experimental data where the key role played in the vertical transport by the miniband width and interface disorder is clearly elucidated.

II. EXPERIMENTAL METHOD

The sample structure is as follows: 1-μm-thick buffer layer, 50 nm of an $Al_xGa_{1-x}As$ layer, superlattice (SL), an enlarged well (EW), superlattice identical to the previous one, 50 nm of an $Al_xGa_{1-x}As$ layer and a 5-nm-thick GaAs caplayer in order to prevent oxidation of the $Al_xGa_{1-x}As$. The two 50-nm-thick $Al_xGa_{1-x}As$ ($x=0.3$) layers were grown to minimize diffusion of the photogenerated carriers into the buffer and to the surface. The active region of the sample is formed by two symmetric superlattices which sandwich the EW. The different samples have 100 periods of an 18/18 superlattice (18-Å-wide wells and barriers, $x=0.3$) with a 40-Å-wide EW in the middle (18/18 sample), 100 periods of a 30/30 superlattice with a 60-Å-wide EW in the middle (30/30 sample), and 50 periods of a 60/60 SL with a 120-Å-wide enlarged well in the middle (60/60 sample). Another set of samples has been grown without the 50-nm-thick $Al_xGa_{1-x}As$ caplayer. The same conclusions as those of Ref. 8 for this kind of sample have been reached: the superlattice dynamics is strongly perturbed by the presence of recombination centers at the free surface and we will not discuss in the following the results obtained for these samples.

The CW experiments have been performed using a Pyridine 2 dye laser pumped by an argon laser. The pho-

toluminescence spectra have been analyzed with a double monochromator (0.1 meV resolution) and recorded by photon counting techniques using a cooled GaAs photomultiplier.

The time-resolved experiments have been performed using a dye laser synchronously pumped by a frequency doubled mode-locked neodymium-doped yttrium-aluminum-garnet (Nd:YAG) laser. The pulse duration was 3 ps and the repetition rate 76 MHz. Pyridine 2 and Styril 9 dyes have been used. The PL signal was dispersed through a monochromator (1 meV resolution) and detected using a synchroscan streak camera. The overall time resolution of the detection system was 20 ps.

The samples were held in a variable temperature cryostat either immersed in helium or under helium flux.

III. EXPERIMENTAL RESULTS

In Table I, the calculated miniband widths for electrons (Δ_e) and heavy holes (Δ_{hh}) have been reported. The three samples present three different situations: (i) both the electronic and heavy-hole minibands are large (18/18 sample), (ii) the electronic miniband is large and the heavy-hole miniband thin (30/30 sample), and (iii) both are thin (60/60 sample).

Figure 1 shows a summary of the experimental data for the 18/18 superlattice. The low-temperature photoluminescence spectrum of the sample recorded under CW excitation is shown in Fig. 1(a). The high-energy peak at $\hbar\omega_{SL} \approx 1.727$ eV is due to the radiative recombination of excitons in the superlattice while the low-energy peak is due to the excitons which recombine in the EW. The disks give the excitation energy ($\hbar\omega_{exc}$) dependence of R, the ratio between the integrated luminescence emission from the EW and the total photoluminescence emission. In a simple model R is proportional to the e-h pair current through the superlattice [see the Appendix, Eq. (A9)]. The ratio R is constant at high energies and decreases as the excitation becomes resonant to $\hbar\omega_{SL}$. We note that for any measured energy the current R is larger than R_L, the ratio between the EW and the EW+SL thicknesses. Assuming that the density of photoexcited pairs is proportional to the layer thickness (the SL absorption coefficient for resonant excitation is 1.5×10^4 cm^{-1}) R_L gives the fraction of e-h pairs directly pho-
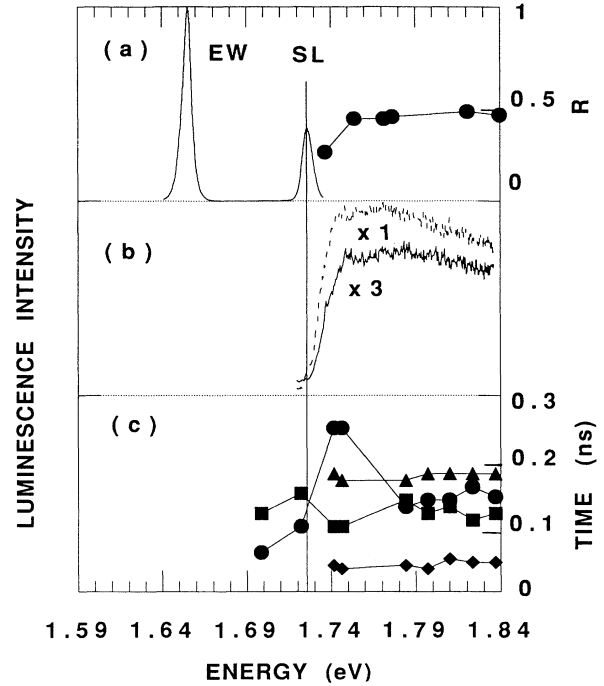
FIG. 1. Summary of the experimental data for the 18/18 superlattice measured at 4 K and with an excitation power of about 1 W cm^{-2}. (a) Photoluminescence spectrum and excitation energy dependence of the ratio (R) between emission I_{EW} from the enlarged well and the total photoluminescence emission. (b) Excitation spectra measured with the detection set at the superlattice (SL) emission (dotted line) and at the enlarged well emission (full line). (c) Decay times (squares and triangles) and rise times (circles and rhombuses) for the EW and for the SL emission, respectively. The lines through the experimental data are only guides for the eyes.

toexcited in the EW with respect to the total number of photoexcited pairs (see Table I).

Increasing the temperature, the ratio R increases up to $\simeq 30$ K, where only luminescence from the EW is detected. The ratio between the luminescence from the enlarged well and the luminescence from the superlattice (R') is proportional to the diffusion coefficient (D) of the e-h pairs [see the Appendix, Eq. (A7)]. Figure 2 shows the results for the three samples studied. At low tem-

TABLE I. Synopsis of the results for the different superlattices: first row, 18/18 superlattice; second row, 30/30 superlattice; third row, 60/60 superlattice. The different columns have the following meanings: R_L is the ratio of the enlarged well thickness to the total thickness of the enlarged well and the superlattice; R is the ratio of the emission intensity from the enlarged well and the total luminescence intensity; Δ_e and Δ_{hh} are the miniband widths for the electrons and for the heavy holes, respectively, calculated using a transfer-matrix approach; $\Delta E_{a/2}$ is the expected energy variation due to half monolayer variations in the well thickness; E_b is the binding energy of the heavy-hole excitons (Ref. 12); ϵ is the activation energy for the e-h pair transport; ΔE_1 (ΔE_2) is the energy difference between the superlattice emission peak and the peak of the excitation spectra for detection set at the SL energy position (EW energy position). ΔE_L is the linewidth of the superlattice emission. The energies are given in meV.

	R_L	R	Δ_e	Δ_{hh}	$\Delta E_{a/2}$	E_b	ϵ	ΔE_1	ΔE_2	ΔE_L
18/18	0.02	0.5	< 134.1	21	21	4	7±1	20	25	7
30/30	0.02	0.2	56.4	1.1	13	4.5	13±2	6	16	6
60/60	0.04	0.1	6.0	< 0.1	4	9	4±1	5	5	2
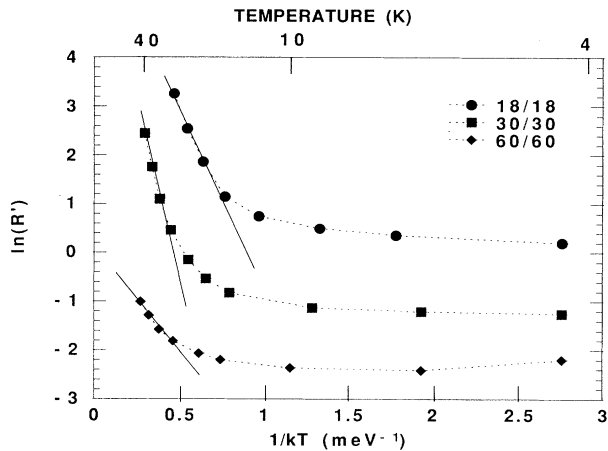
FIG. 2. Temperature dependence of R', the ratio between the integrated photoluminescence from the enlarged well and the superlattice, for the 18/18 superlattice (disks), the 30/30 superlattice (squares), and the 60/60 superlattice (rhombuses). The high-temperature data have been fitted using an activationlike dependence (full lines) whose parameters are reported in Table I. The excitation energy is 1.95 eV and the excitation power is 1 W cm^{-2}.

perature, R' is almost constant; increasing the temperature ($T > 20$ K), R' presents an activationlike behavior. From the slope of R' versus the inverse temperature in a semilog plot, the activation energy ϵ has been deduced (see the table). We have assumed, as usual, that ϵ corresponds to the characteristic energy which separates the localized and the delocalized states.[9]

The dependence of R from the excitation power J_{exc} is shown in Fig. 3. Increasing J_{exc}, R first decreases, goes through a minimum at an e-h pair density around 6×10^{11} cm^{-3}, and eventually increases.

The low-temperature luminescence excitation spectra
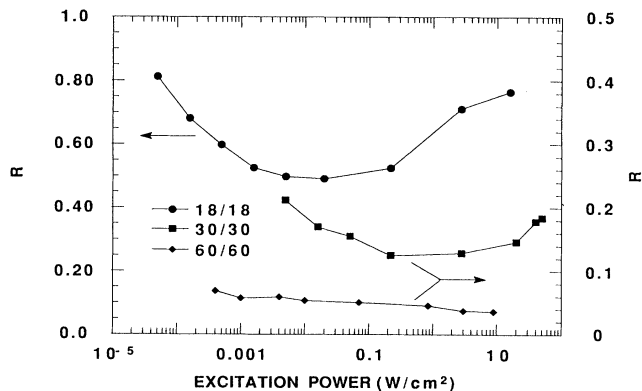
FIG. 3. Excitation power dependence of the current R through the superlattice for the 18/18 superlattice (disk), the 30/30 superlattice (squares), and the 60/60 superlattice (rhombuses), where $R = I_{EW}/(I_{EW} + I_{SL})$ and I_{EW}, I_{SL} are the integrated photoluminescence from the enlarged well and the superlattice, respectively. The lines are only guides for the eyes. The excitation energy is 2.5 eV.

measured with the detection energy fixed at the EW emission energy (full curve) and with the detection energy fixed at $\hbar\omega_{SL}$ (dashed curve) are shown in Fig. 1(b).[10] Clearly resolved excitonic peaks are absent both in the EW and the SL excitation spectrum. The overall spectral shape is steplike and very similar in both cases although the onset region in the SL excitation spectrum is shifted to higher energies than in the EW excitation spectrum. This shift can be quantified by measuring the energy difference between $\hbar\omega_{SL}$ and the edge of the SL excitation spectrum (defined in Table I as ΔE_1) and between $\hbar\omega_{SL}$ and the edge of the EW excitation spectrum (defined in Table I as ΔE_2).

In Fig. 1(c) the information that we have extracted from the time-resolved luminescence measurements are summarized. For $\hbar\omega_{ex}$ lower than 1.74 eV the superlattice is almost transparent and all the e-h pairs are directly created inside the EW. The dynamics are characteristics of the isolated EW studied and the observed rise time is only connected to the cooling of the excited pairs. The time dependence of the luminescence signal has been fitted by assuming a three-level model (see the Appendix and Fig. 7) and two characteristic times have been extracted: the rise time (τ_r^{EW}, disks in Fig. 1) and the decay time [τ_d^{EW}, filled squares in Fig. 1(c)] of the EW photoluminescence. By increasing $\hbar\omega_{exc}$ above $\hbar\omega_{SL}$, e-h pairs begin being generated in the superlattice; they partly recombine in the SL region with two characteristic times (τ_r^{SL} rhombuses and τ_d^{SL} triangles), while the others diffuse and eventually reach the EW where they recombine. For $\hbar\omega_{exc} > \hbar\omega_{SL}$, the main contribution to the EW photoluminescence comes from the e-h pairs photoexcited in the SL which diffuse into the EW (see the excitation spectra). Thus, τ_r^{EW} jumps from about 60 ps to 240 ps while τ_r^{EW} stays almost constant at 120 ps. The increase in τ_r^{EW} is connected with the diffusion of e-h pairs through the SL. The constancy of τ_d^{EW} indicates that the recombination dynamics of the EW is not perturbed by the origin of the e-h pairs (transport or direct photexcitation). Increasing still further $\hbar\omega_{exc}$, τ_r^{EW} decreases to about 120 ps. If the excitation energy is resonant with $\hbar\omega_{SL}$, even though e-h pairs are generated in the SL, τ_r^{EW} is the same as when we excite directly in the EW ($\hbar\omega_{exc} < \hbar\omega_{SL}$). The spectral dependence of τ_r^{EW} reflects the energy dependence of the EW excitation spectrum, i.e., is characteristic of the transport properties of the excited e-h pairs. The recombination dynamics of the SL is almost independent on $\hbar\omega_{exc}$.

Similar sets of experimental data have been collected for the other samples as well. Figure 4 and Table I (second row) present a summary of the experimental data for the 30/30 sample. In a 6-nm period superlattice, the heavy-hole miniband shrinks to about 1 meV. This strongly inhibits the vertical heavy-hole diffusion. Indeed for high excitation energies R=0.5 for the 18/18 superlattice and R=0.2 for the 30/30 superlattice, while R_L is the same in both cases.

The photoluminescence spectrum of sample 30/30 is shown in Fig. 4(a). The e-h pair current R presents a minimum for $\hbar\omega_{exc}$ resonant with the SL luminescence peak. The dependence of R' on T (filled squares in Fig.
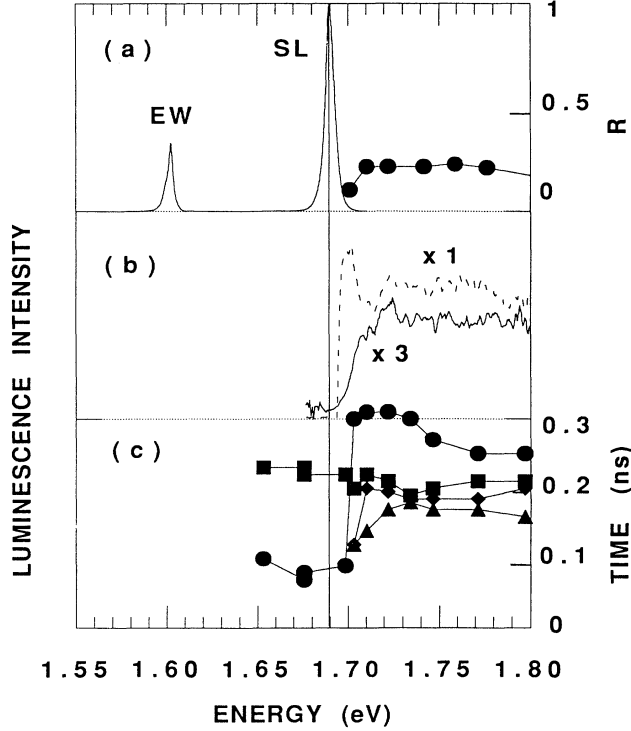
FIG. 4. Summary of the experimental data for the 30/30 superlattice measured at 4 K and with an excitation power of about 1 W cm^{-2}. The different panels and symbols have the same meanings as those in Fig. 1.

FIG. 5. Summary of the experimental data for the 60/60 superlattice measured at 4 K and with an excitation power of about 1 W cm^{-2}. The different panels and symbols have the same meanings as those in Fig. 1.

2) has a very similar shape to that observed for the 18/18 sample, with a different value of ϵ (13 meV). In Fig. 3 (filled squares) we show the power dependence of R for this sample: increasing J_{exc}, R starts decreasing, reaches a minimum for an excited e-h pair density of $\simeq 6 \times 10^{13}$ cm^{-3}, and then increases.

Depending on the detection energy, different excitation spectra are measured [see Fig. 4(b)]. The SL excitation spectrum presents at high energy a peak associated to the SL heavy-hole exciton with a Stokes shift of $\Delta E_1 = 6$ meV. The SL light-hole exciton resonance is at about 1.725 eV. The EW excitation spectrum has a different shape for $\hbar\omega_{\text{exc}}$ in the heavy-hole superlattice regions. The line shape looks now very similar to that of the 18/18 SL. No heavy-hole excitonic peak is measured but instead a steplike onset. For the light-hole exciton region, the two excitation spectra are similar indeed. The temporal dynamics of the e-h pairs in this sample is summarized in Fig. 4(c). For $\hbar\omega_{\text{exc}} < \hbar\omega_{\text{SL}}$, $\tau_r^{\text{EW}} \simeq 80$ ps; for $\hbar\omega_{\text{exc}} \geq \hbar\omega_{\text{SL}}$, $\tau_r^{\text{EW}} \simeq 300$ ps; and for higher $\hbar\omega_{\text{exc}}$, $\tau_r^{\text{EW}} \simeq 250$ ps. The energy dependence of τ_r^{EW} is very similar to that of the EW excitation spectrum and differs from the SL excitation spectrum which is related to the absorption coefficient in the SL.

Figure 5 and Table I (third row) report the summary of the experimental data for the 60/60 superlattice which is characterized by a very thin miniband for both the electrons and the heavy holes. Based on the previous discussion we expect a very weak vertical transport. Indeed

$R = 0.1 \simeq R_L$ (see the table). Figure 3 (rhombuses) reports the power dependence of R for this sample. No minimum in R is apparent, only a smooth decreases as J_{exc} increases. R depends very weakly on the temperature, passing from 0.1 at 4 K to 0.25 at 44 K. An activationlike dependence of R' on T has been tentatively fitted for this sample in the high-temperature range (Fig. 2). The SL and EW excitation spectra [see Fig. 5(c)] increase with the excitation energy in the same way. A first peak is observed at 1.605 eV and then another strong peak at 1.628 eV. We attribute these peaks to the absorption of the heavy- and light-hole excitons in the superlattice, respectively.[11] The measured light-hole–heavy-hole exciton energy splitting is about 23 meV, which is in reasonable agreement with similar values found for symmetric superlattices in Ref. 12. The temporal decays of the PL from the EW and SL have been measured also for this sample and the same behavior discussed for the other samples is observed. At $\hbar\omega_{\text{exc}} \simeq \hbar\omega_{\text{SL}}$, τ_r^{EW} passes from 200 ps to 600 ps and increasing $\hbar\omega_{\text{exc}}$ still further, it assumes a value of 400 ps, while the other time constants remain almost stable at about 200 ps.

IV. DISCUSSION

The different results for the three samples can be explained in terms of the different properties of the vertical transport. Let us try to review and discuss the main ex-

perimental features presented in the preceding section. We would like, however, to premise a few key points upon which the whole discussion is based. First of all, we will assume that no sizable charge buildup within the superlattice is originated by the photogenerated carriers as a consequence of the small carrier densities used in the measurements ($n_{eh} \leq \times 10^{15}$ cm^{-3}, where n_{eh} is the density of photoexcited e-h pairs), in agreement with Refs. 13 and 14. As far as the carrier transfer into the enlarged well is concerned, we will assume again that no charge accumulation at the EW interfaces will result in the short period SL samples (18/18 and 30/30) because of effective-mass filtering effects.[15] In fact, carrier tunneling through thin barriers is always so fast that no luminescence is usually observed from narrow wells in asymmetric coupled quantum-well structures for barrier thicknesses up to 30–35 Å.[13,15,16] We can therefore exclude major influence on carrier diffusion due to charge buildup at the EW interfaces and, at the same time, safely interpret the rise time of the PL from the EW for $\hbar\omega_{\mathrm{exc}} \geq \hbar\omega_{\mathrm{SL}}$ in terms of vertical transport effects. A different situation might occur in the 60/60 sample; in this case the vertical transport has been found to be very inefficient and much longer rise times in the PL decay curves are expected with possible contributions from the non-negligible transfer times into the enlarged well. We will therefore focus the main part of the discussion to the short period SL samples.

The dependence of R on the excitation power shows two typical behaviors: a decrease at low powers and an increase at high powers. The transition between the two is sample dependent: $n_{eh} \simeq 6 \times 10^{11}$ cm^{-3} for the 18/18 sample and $n_{eh} \simeq 6 \times 10^{13}$ cm^{-3} for the 30/30 sample. A slow decrease is instead observed for the 60/60 sample up to the highest density used, $n_{eh} \simeq 5 \times 10^{14}$ cm^{-3}.

The decrease of R can be interpreted as a change from electronic to ambipolar transport when increasing n_{eh}.[17] In fact, GaAs/Al$_x$Ga$_{1-x}$As superlattices have a weak residual p-type doping (N_A), where the acceptors are all frozen at low temperature and in the dark. Under optical illumination the situation changes: the neutrality condition requires that the density of holes balance the density of electrons plus the density of ionized acceptors:

$$N_A^- + n_e = n_h. \tag{1}$$

For $n_{eh} < N_A$ the photoexcited electrons are minority carriers. They diffuse through the SL and recombine in the EW with the holes present there due to the residual doping. On the contrary, if $n_{eh} > N_A$, electrons have to wait for the heavy-hole arrival in order to recombine inside the EW. Hence for $n_{eh} > N_A$ the transport is ambipolar and dominated by the heavy-hole diffusion.

We believe that the rise in R when further increasing n_{eh} is due to the saturation of the nonradiative channels in the EW. In fact,

$$\frac{1}{\tau_{\mathrm{EW}}} = \frac{1}{\tau_{\mathrm{rad}}} + \frac{1}{\tau_{\mathrm{nrad}}}, \tag{2}$$

where τ_{EW} is the EW recombination time, τ_{rad} and τ_{nrad} are the radiative and nonradiative recombination time, and

$$I_{\mathrm{EW}} = I_0 \frac{\tau_{\mathrm{EW}}}{\tau_{\mathrm{rad}}} = I_0 \eta \tag{3}$$

where I_{EW} is the luminescence intensity, I_0 a normalization factor that depends on the number of the photocreated carriers, and η in the radiative efficiency. If τ_{nrad} decreases and τ_{rad} remains constant the efficiency increases. Thus R increases due to an increase of the nonradiative lifetime in the EW. This fact also explains the sample dependence of the critical density at which R starts increasing: due to a higher transport in the case of the 18/18 sample, a lower excitation intensity is needed to generate a sufficiently high e-h pair density in the EW to saturate the nonradiative channels. The transport is less efficient in the 30/30 sample and hence the critical density is higher. Finally for the 60/60 sample, which shows a very inefficient transport, the critical density is never reached under our experimental conditions.

The temperature dependence of R' is explained with a temperature activation of localized states which are present in the SL.[9] At low temperatures R' remains constant up to a temperature which is high enough to overcome the energy difference between the localized states and the extended ones. For higher temperatures, R' increases because more and more e-h pairs in the localized states are thermally promoted to the extended states. The onset region is smooth, indicating somehow a spreading in the activation energies through the superlattice. For the 60/60 sample, the increase observed in R' at high temperatures is indicative of the onset of this regime and the value of ϵ extracted from the data cannot be interpreted anymore in terms of an activation energy. Consequently, at 4 K the transport is dominated by hopping between localized states and is not a Bloch transport. In particular, the Bloch transport presents a different temperature behavior: namely, it decreases when increasing the temperature because of the increase in the scattering.[18] Our findings are not in contrast with the data of Ref. 19, where a Bloch conduction is found in SL with a period shorter than 20/20. In fact, those measurements have been done at higher excitation than in our experiments and at 16 K. In Fig. 2, 16 K corresponds to the onset of the thermally activated delocalized transport for the 18/18 sample.

The main results of the time-resolved luminescence experiments can be summarized as follows.

(1) The rise time of the EW luminescence increases when the excitation energy is higher than the SL absorption edge, indicating a contribution from the transport to τ_r^{EW}.

(2) Varying $\hbar\omega_{\mathrm{exc}}$, the rise time of the EW luminescence increases as $\hbar\omega_{\mathrm{exc}}$ becomes resonant with the SL luminescence energy. This indicates that the transport is less effective for these energies, and, therefore, the presence of localized states in the superlattice. In particular, the EW rise time is connected with the diffusion constant of the e-h pairs. In the transition region between localized and extended states, the mobility of a disordered system decreases and smoothly tends to zero for energies lower than the energy of the mobility edge.[9] The rise time of the EW luminescence follows this trend: it increases as

the excitation energy approaches the SL emission energy and decreases to the value measured in the absence of direct excitation of the superlattice as the excitation energy is resonant with the SL emission energy indicating a null transport of these states.

(3) For $\hbar\omega_{\text{exc}} \gg \hbar\omega_{\text{SL}}$, the EW rise time becomes longer and longer when increasing the period of the superlattice (150 ps for the 18/18 sample, 250 ps for the 30/30 sample, and 450 ps for the 60/60 sample). This is directly connected with the different miniband width which induces a lower transport as the SL period increases.

(4) The SL rise time is about 200 ps for all samples. A similar time has been found in Ref. 20 and interpreted as the time for the exciton relaxation to $\mathbf{k} = 0$.

(5) The SL decay time is about 50 ps for the 18/18 sample and about 200 ps for the other samples. This is due to the fact that in the 18/18 sample the dominant "recombination" mechanism is the trapping into the EW, while for the other samples radiative recombination in the SL region dominates.

(6) In the simple model given in the Appendix, the rise times of the EW and SL photoluminescence turn out to be equal and determined by the thermalization time into the SL and the transfer time into the EW [see Eqs. (A10) and (A11)]. However, the measured times are different. In particular, the temporal dynamics in the SL does not depend on the transport efficiency, i.e., on $\hbar\omega_{\text{exc}}$. More complicated models which include hopping conduction between localized states, exciton formation in the EW, trapping and detrapping of excitons in the superlattices, seem therefore to be needed in order to fully reproduce the experimental data.

As a consequence of our experimental observations two parameters seem to play a key role in determining the kind of transport: the width of the superlattice minibands and the amount of disorder present in the samples. A schematic diagram of the pair density of states including both aspects is shown in Fig. 6. The luminescence at energy $\hbar\omega_{\text{SL}}$ is due to radiative recombinations of localized excitons in the SL (when we excite in resonance with $\hbar\omega_{\text{SL}}$ the transport, and hence R, diminishes). Due to the thermalization processes, $\hbar\omega_{\text{SL}} - \Delta E_L/2$ is the energy of the edge of the excitonic states broadened by the disorder (ΔE_L is the full width at half maximum of the superlattice photoluminescence peak). The peak energy of the excitonic band is given by the energy of the peak associated to the SL excitons, i.e., the excitonic position is given by $\hbar\omega_{\text{SL}} + \Delta E_1$. This energy corresponds to the excitonic energy in the absence of the disorder or other broadening mechanism, $E_x = E_g + E_e + E_{\text{hh}} - E_b = \hbar\omega_{\text{SL}} + \Delta E_1$ where E_g is the GaAs band-gap energy, E_e and E_{hh} are the confinement energies for the electrons and for the heavy holes, and E_b is the binding energy of the excitons. Using the values for E_b obtained from Ref. 12 and reported in Table I we can find the energy of the edge of the continuum of the e-hh pair density of states, $E_{e\text{-hh}}$. The activation energy is the energy which separates the localized states and the extended states, consequently the mobility edge (E_μ) will be at $E_\mu = \hbar\omega_{\text{SL}} - \Delta E_L + \epsilon$.

If we apply this model to the samples investigated we
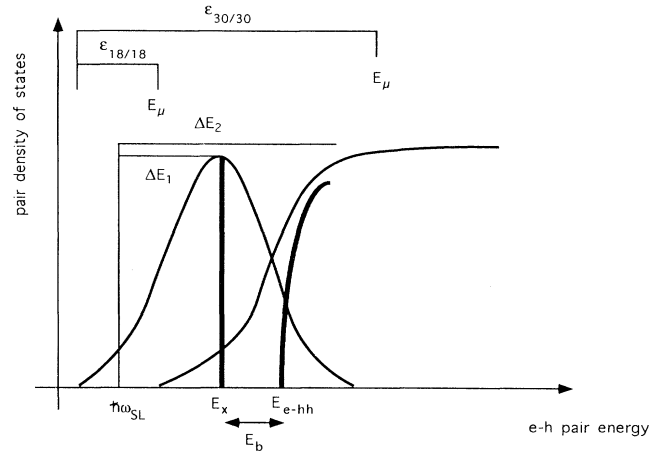
FIG. 6. Schematic diagram of the pair density of states deduced by the experimental data. The thick lines refer to the no-disorder case, while the thin ones include the broadening due to disorder. E_{SL} is the peak energy of the superlattice emission, E_x the heavy-hole excitonic energy, E_b the exciton binding energy, $E_{e\text{-hh}}$ the energy of the continuum edge of dissociated heavy-hole–electron pair, ΔE_1 (ΔE_2) the energy difference between the superlattice emission peak and the peak of the excitation spectra for the detection set at the SL energy position (EW energy position); $\epsilon_{n/n}$ the activation energy for the diffusion constant of the n/n superlattice; E_μ the mobility edge.

find two different situations: $E_\mu < E_{e\text{-hh}}$ for the 18/18 sample, while $E_\mu > E_{e\text{-hh}}$ for the 30/30 and 60/60 samples. This difference can indeed explain the different properties of the vertical transport in the different samples.

The difference between the SL excitation spectrum and the EW excitation spectrum for the 18/18 Å superlattice is due to the small energy difference between the localized and the delocalized states as measured by the activation energy ϵ. In this case $\epsilon \simeq \Delta E_2 - \Delta E_1$. The large Stokes shift between the PL and the SL excitation spectrum is due to the fact that for such a small superlattice period the variation in thickness of half a monolayer results in a large variation in the confinement energy. Indeed, increasing the temperature, $\hbar\omega_{\text{SL}}$ shifts towards higher energies and not to lower energies as the band-gap thermal shrinkage would suggest. This is due to the thermal population of higher-energy states. The absence of a well-resolved excitonic peak in the excitation spectra is mainly due to two effects: the interface fluctuations, that broaden the excitonic peak, and the negligible influence of the excitation energy on the transport properties, which keeps the shape of the excitation spectra flat.[8]

In the 30/30 sample the SL excitation spectrum follows the joint density of states for energies below E_μ, where the transport is not efficient, and decreases at higher energies. This allows the observation of a clear excitonic peak in the SL excitation spectrum. The EW excitation spectrum presents its onset at the energy $\hbar\omega_{\text{SL}} + \Delta E_2$, corresponding, to a good approximation, to E_μ where the mobility starts increasing. The light-hole resonance

peak is present in both spectra, indicating that light-hole excitons also contribute to the transport.

V. CONCLUSION

A consistent picture seems to emerge from the whole set of experimental data. At low temperature (4 K), the transport occurs by hopping between localized states in all our samples. If the period of the superlattices is short, about 4 nm, and the miniband width is large (>10 meV) for both electrons and heavy holes, the localization can be related to the disorder produced by the interface fluctuations. Increasing the temperature, a Bloch transport of correlated e-h pairs is activated.

In intermediate period superlattices, with a period of about 6 nm, the electron miniband is large, but the heavy-hole miniband width is less than 2 meV. The hopping occurs between excitons not necessarily localized by the disorder fluctuations; in fact, the superlattice acts as a sequence of isolated quantum wells for the heavy holes. Increasing the temperature, a Bloch transport is activated if the exciton thermal dissociation starts allowing the independent motion of uncorrelated e-h pairs.

Finally, if the period of the superlattice is greater than 12 nm, both electrons and holes are strongly confined inside the wells and substantially no transport takes place.

ACKNOWLEDGMENTS

APPENDIX

In this appendix we describe the simple set of rate equations used to extract the pair diffusion coefficient D from the time integrated luminescence spectra and the different time constants from the time-resolved luminescence spectra. A schematic sketch is given in the inset of Fig. 7. Let us define n_{SL}, n_{SL}^{exc}, and n_{EW} the density of free electron-hole pairs in the SL, the density of excitons in the SL, and the density of e-h pairs (free and bound) in the EW, respectively. In addition, we call τ_{tr} the average time for a free e-h pair generated in the SL to arrive in the EW, τ_{th} the time for an e-h pair to relax and form an exciton in the SL, τ_{SL} and τ_{EW} the recombination times for excitons in the SL and in the EW, and $P(t)$ the e-h pair density generated by the laser pulse assuming a homogeneous excitation. We approximate the free e-h pair temporal dynamics in the superlattice with a generation term $L_{SL}/(L_{EW}+L_{SL})P(t)$, a thermalization term $-n_{SL}/\tau_{th}$, and a term which gives the trapping into the enlarged well $-n_{SL}/\tau_{tr}$. Consequently, the superlattice exciton rate equation contains a generation term n_{SL}/τ_{th} and a recombination term $-n_{SL}^{exc}/\tau_{SL}$. Analogously in the enlarged well, we have a generation term which includes the direct excitation and the spill over from the superlattice $[L_{EW}/(L_{EW}+L_{SL})P+n_{SL}/\tau_{tr}]$ and a recombination term $-n_{EW}/\tau_{EW}$. Finally, we obtain a system of three coupled differential equations:
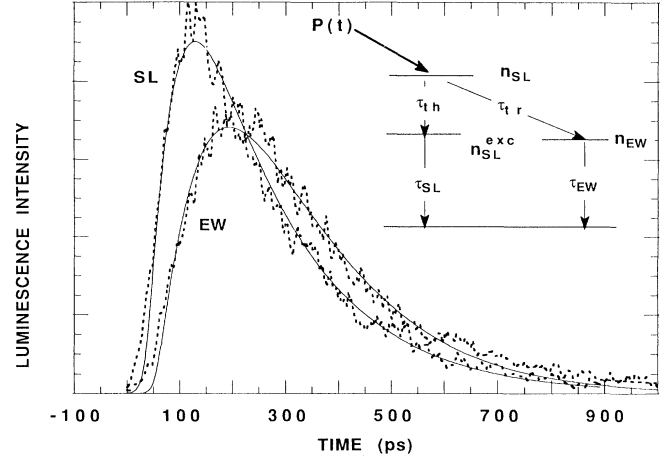
FIG. 7. Time-resolved luminescence intensities at 4 K for the 30/30 sample. The dotted line is related to luminescence coming from SL and the continuous line to luminescence coming from EW. A sketch the model used for the fit is reported in the onset, and explained in the Appendix.

$$\frac{dn_{SL}}{dt} = \frac{L_{SL}}{L_{EW}+L_{SL}}P(t) - \frac{n_{SL}}{\tau_{th}} - \frac{n_{SL}}{\tau_{tr}} , \qquad (A1)$$

$$\frac{dn_{SL}^{exc}}{dt} = \frac{n_{SL}}{\tau_{th}} - \frac{n_{SL}^{exc}}{\tau_{SL}} , \qquad (A2)$$

$$\frac{dn_{EW}}{dt} = \frac{L_{EW}}{L_{EW}+L_{SL}}P(t) + \frac{n_{SL}}{\tau_{tr}} - \frac{n_{EW}}{\tau_{EW}} . \qquad (A3)$$

Let us first consider stationary excitation conditions $P(t) = P$. The time integrated luminescence I from the superlattice and the enlarged well can be approximated by $I_{SL} = n_{SL}^{exc}/\tau_{SL}$ and $I_{EW} = n_{EW}/\tau_{EW}$, respectively. We solve Eqs. (A1)–(A3) considering that the density of e-h pairs directly photoexcited in the EW is negligible compared to the density of e-h pairs which from the SL spill into the EW. Using Eqs. (A1)–(A3) and the definition

$$R' = \frac{I_{EW}}{I_{SL}} = \frac{n_{EW}\tau_{SL}}{\tau_{EW}n_{SL}^{exc}} , \qquad (A4)$$

we can correlate the measured values of R' to τ_{tr}:

$$\frac{1}{\tau_{tr}} = \frac{1}{\tau_{th}}R' . \qquad (A5)$$

From the knowledge of the transfer time, τ_{tr}, it is therefore possible to extract from the experimental data the diffusion constant D, and the e-h pair current, J. In fact, to be trapped into the EW an e-h pair generated in the SL has to cross a distance of the order of L_{eff}, where

$$L_{eff} = \frac{1}{L_{SL}} \int_0^{L_{SL}} z \exp(-\alpha z) \, dz. \qquad (A6)$$

Hence we can assume for D:

$$D \equiv \frac{L_{eff}^2}{\tau_{tr}} = \frac{L_{eff}^2}{\tau_{th}}R' . \qquad (A7)$$

As far as the current is concerned we assume that the number of e-h pairs which arrive in the EW per unit time is $J \equiv q v_{SL} n_{SL}$, where q is the electrical charge and $v_{SL} \simeq L_{eff}/\tau_{tr}$. From Eq. (A1), one finds for n_{SL} $(L_{SL} \gg L_{EW})$

$$n_{SL} \simeq P \frac{\tau_{th}\tau_{tr}}{\tau_{th} + \tau_{tr}} , \qquad (A8)$$

which yields for J

$$J = qL_{eff}PR , \qquad (A9)$$

where $R = I_{EW}/(I_{EW} + I_{SL})$ is an experimental quantity.

Within these approximations, R differs from the current J only for a constant factor. Moreover, the diffusion coefficient D is proportional to R', with τ_{th} entering in the proportionality factor. The thermalization depends on the interaction of the e-h pairs with the lattice via acoustic phonons scattering and scattering by defects such as interface fluctuations or impurities. Scattering with defects is known to be independent on the temperature, while acoustic phonon scattering depends linearly on the temperature.[20] In the temperature interval that we investigate (4–30 K) the thermalization time may change only by a factor of about 5,[21] which is negligible with respect to a change of three or four orders

of magnitude in R'. Hence, from the photoluminescence spectra as a function of the temperature, we can infer the temperature dependence of the superlattice diffusion constant.

Figure 7 shows typical experimental decay spectra (dotted lines) of the photoluminescence collected from the EW and the SL for excitation energies higher than $\hbar\omega_{SL}$. For the analysis of the time decay of the luminescence we have used the set of rate equations given by Eqs. (A1)–(A3). Supposing again a negligible direct generation in the EW, we can solve the equations for a Δ-like excitation, $P(t) = P_0 \delta(t)$, and obtain

$$n_{SL}^{exc}(t) = P_0 \frac{\Gamma_{th}}{\Gamma_{SL} - (\Gamma_{th} + \Gamma_{tr})}$$
$$\times \{\exp[-(\Gamma_{th} + \Gamma_{tr})t] - \exp(-\Gamma_{SL}t)\}, \quad (A10)$$
$$n_{EW}(t) = P_0 \frac{\Gamma_{tr}}{\Gamma_{EW} - (\Gamma_{tr} + \Gamma_{th})}$$
$$\times \{\exp[-(\Gamma_{th} + \Gamma_{tr})t] - \exp(-\Gamma_{EW}t)\}, \quad (A11)$$

where $\Gamma_i = 1/\tau_i$. We have therefore fitted the PL decay curves as the difference of two exponentials, the shorter time characterizing the PL rise and the longer one the PL decay (see the full lines in Fig. 7). In fact, we have not forced the arguments of the first two exponentials to be equal given the crudeness of the model.

*On leave from Departament de Fisica Aplicada, Universitat de Valencia, 46100 Burjassot, Valencia, Spain.

[1] A. Chomette, B. Deveaud, J. Y. Emery, and A. Regreny, Superlatt. Microstruct. 1, 201 (1985).

[2] F. Capasso, K. Mohammed, and A. Cho, IEEE J. Quantum Electron. QE-22, 1853 (1986).

[3] A. Chomette, B. Deveaud, J. Y. Emery, A. Regreny, and B. Lambert, Solid State Commun. 54, 75 (1985).

[4] A. Chomette, B. Deveaud, A. Regreny, and G. Bastard, Phys. Rev. Lett. 57, 1464 (1986).

[5] E. Tuncel and L. Pavesi, Philos. Mag. B 65, 213 (1992).

[6] A. Chomette, B. Deveaud, B. Lambert, F. Clerot, and A. Regreny, Superlatt. Microstruct. 5, 565 (1989).

[7] J. Puls, F. Henneberg, I. N. Uraltsev, and A. M. Vassiliev, Superlatt. Microstruct. 9, 503 (1991).

[8] A. Chomette, B. Lambert, B. Clerjaud, F. Clerot, H. W. Liu, and A. Regreny, Semicond. Sci. Technol. 3, 351 (1988).

[9] N. F. Mott and E. A. Davies, *Electronic Processes in Non-Crystalline Materials* (Clarendon, Oxford, 1979).

[10] The excitation spectrum is the product of the joint density of states times a thermalization function from $\hbar\omega_{exc}$ to the state from which the luminescence is collected. In the case of quantum wells, one usually assumes that the thermalization function depends very weakly on the energy and hence the excitation spectrum is representative of the absorption coefficient. In a superlattice this is true in the absence of vertical transport. If traps are present in the superlattice, the energy dependence of the thermalization function to the traps (in this case it is better to speak about the transfer function which is indicative of the vertical transport) should be taken into account. In our samples the EW acts as a trap, and consequently the EW excitation spectra give information about the states that contribute to the transport (an e-h pair is created at energy $\hbar\omega_{exc}$ in the superlattice and

recombines at the energy of the EW), while the SL excitation spectrum measures the density of states from which the e-h pairs recombine directly in the superlattice region (Refs. 3 and 8).

[11] Usually, in superlattices, it is found that the heavy-hole excitonic resonance has a comparable strength to the light-hole excitonic resonance (see Fig. 4). This is not the case for our samples. At the moment we miss the reason. Experimentally we have found on other superlattices as well as with different periods that the intensity of the excitonic resonances is strongly dependent on the detection energy. A detailed theory of the photoluminescence excitation line shape in superlattices and quantum wells is highly desirable.

[12] A. Chomette, B. Lambert, B. Deveaud, F. Clerot, A. Regreny, and G. Bastard, Europhys. Lett. 4, 461 (1987).

[13] R. Sauer, K. Thonke, and W. T. Tsang, Phys. Rev. Lett. 61, 609 (1988).

[14] S. Tarucha and K. Ploog, Phys. Rev. B 38, 4198 (1988).

[15] D. H. Levi, D. R. Wake, M. V. Klein, J. Kumar, and H. Morkoç, Phys. Rev. B 45, 4274 (1992).

[16] P. Roussignol, M. Gurioli, L. Carraresi, M. Colocci, A. Vinattieri, and C. Deparis, Superlatt. Microstruct. 9, 151 (1991).

[17] B. Lambert, B. Deveaud, A. Chomette, A. Regreny, and B. Sermage, Semicond. Sci. Technol. 4, 513 (1989).

[18] B. Lambert, B. Deveaud, A. Chomette, F. Clerot, A. Regreny, and B. Sermage, Surf. Sci. 228, 446 (1990).

[19] B. Deveaud, J. Shah, T. C. Damen, B. Lambert, and A. Regreny, Phys. Rev. Lett. 58, 2582 (1987).

[20] T. C. Damen, J. Shah, D. Y. Oberli, D. S. Chemla, J. E. Cunningam, and J. M. Kuo, Phys. Rev. B 42, 7434 (1990).

[21] P. Roussignol, C. Delalande, A. Vinattieri, L. Carraresi, and M. Colocci, Phys. Rev. B 45, 6965 (1992).